JACS
JOURNAL OF THE AMERICAN CHEMICAL SOCIETY
pubs.acs.org/JACS
Article

Mechanism and Origin of Remote Stereocontrol in the Organocatalytic Enantioselective Formal C(sp^2)−H Alkylation Using Nitroalkanes as Alkylating Agents

Sharath Chandra Mallojjala, Rahul Sarkar, Rachael W. Karugu, Madhu Sudan Manna, Sayan Ray, Santanu Mukherjee,* and Jennifer S. Hirschi*

Cite This: J. Am. Chem. Soc. 2022, 144, 17399−17406
Read Online
ACCESS | Metrics & More | Article Recommendations | Supporting Information

ABSTRACT: Experimental ^{13}C kinetic isotope effects (KIEs) and density functional theory (DFT) calculations are used to evaluate the mechanism and origin of enantioselectivity in the formal C(sp^2)−H alkylative desymmetrization of cyclopentene-1,3-diones using nitroalkanes as the alkylating agent. An unusual combination of an inverse (~0.980) and a normal (~1.033) KIE is observed on the bond-forming carbon atoms of the cyclopentene-1,3-dione and nitroalkane, respectively. These data provide strong support for a mechanism involving reversible carbon−carbon bond formation followed by rate- and enantioselectivity-determining nitro group elimination. The theoretical free-energy profile and the predicted KIEs indicate that this elimination event occurs via an E1cB pathway. The origin of remote stereocontrol is evaluated by distortion−interaction and SAPT0 analyses of the E1cB transition states leading to both enantiomers.

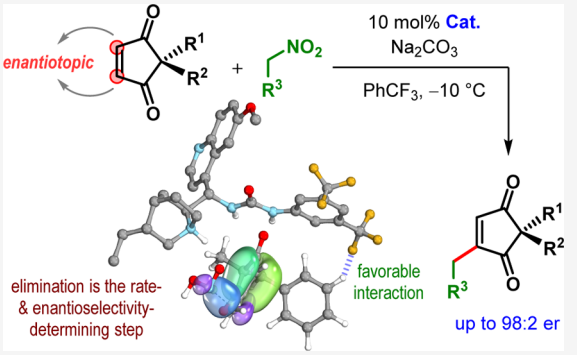

INTRODUCTION

Direct functionalization of a specific C−H bond from a diverse ensemble of C−H bonds present in an organic molecule is arguably the most efficient and economic route for generating molecular complexity.[1] The past decade has witnessed tremendous growth in the area of transition metal-catalyzed direct C−H activation,[2−4] mostly with the help of strategically placed directing groups.[5,6] These approaches have often led to site selectivities unthinkable using conventional chemistry.[7] Despite continuing developments of transition metal-catalyzed C−H activation reactions, functionalization of olefinic C-(sp^2)−H bonds appears to be far more challenging when compared to aromatic C(sp^2)−H bonds. Moreover, introduction of an unfunctionalized alkyl group (e.g., methyl) into a specific C(sp^2)−H bond remained elusive.[8,9] An additional level of difficulty arises when the C−H bond functionalization in question results in the generation of a stereocenter and the issue of enantiocontrol comes into the picture.[10,11]

In 2015, one of our groups developed a simple strategy[12] for formal introduction of unfunctionalized alkyl groups into olefinic C(sp^2)−H bonds not only enantioselectively but also without using a directing group. This transformation utilizes air-stable and inexpensive nitroalkanes (**2**) as the alkyl source under the influence of a bifunctional tertiary aminourea derivative (**4**) as the catalyst (Scheme 1A). More specifically, prochiral 2,2-disubstituted cyclopentene-1,3-diones (e.g., **1**) were desymmetrized enantioselectively through formal C-(sp^2)−H alkylation. The generality of this strategy was subsequently demonstrated for the enantioselective desymmetrization of *meso*-norbornenoquinones[13] and recently applied to the enantioselective total synthesis of [3]-ladderanol.[14] These transformations do not lead to the creation of any stereocenter at the reaction site but allow for the generation of stereocenter(s) remote from the reaction site—a phenomenon often termed as remote stereocontrol.[15] While the initial findings have already led to the development of other transformations[16,17] and applied to the enantioselective synthesis of complex targets,[14] a detailed mechanistic study of this reaction holds the potential to unearth valuable information.

As a preliminary hypothesis, an enantioposition-selective conjugate addition of **2** to **1** was proposed to form the initial carbon−carbon bond. Elimination of the nitro group from this ensuing adduct followed by isomerization presumably leads to formation of the desymmetrized product **3** (Scheme 1B). This addition−elimination−isomerization sequence likely occurs in

Received: March 17, 2022
Published: September 15, 2022

https://doi.org/10.1021/jacs.2c02941
J. Am. Chem. Soc. 2022, 144, 17399−17406

Scheme 1. (A) Bifunctional Urea-Catalyzed Enantioselective Desymmetrization via Formal C(sp²)−H Alkylation;[12] (B) Originally Proposed Pathway and Outstanding Mechanistic Questions Addressed in This Study

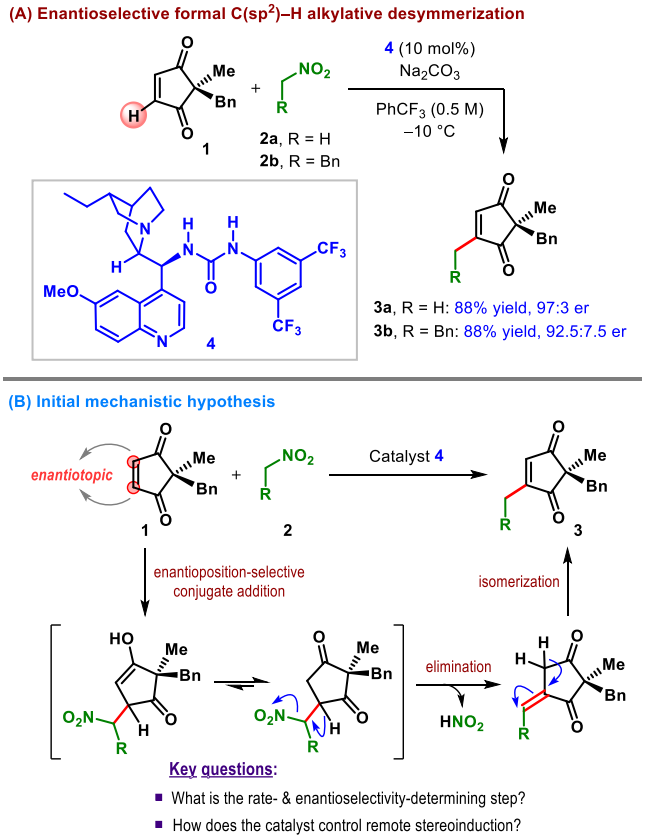

the chiral pocket of the dihydroquinine-derived urea catalyst **4**. However, it is not immediately obvious which of the above steps is responsible for the origin of enantioselectivity observed in this reaction. Identification of the first irreversible step in the catalytic cycle is critical to obtain insights into how this bifunctional chiral urea orchestrates remote stereocontrol in this reaction.

RESULTS AND DISCUSSION

In the modern era, density functional theory (DFT) calculations are widely employed in elucidating reaction mechanisms. DFT calculations in combination with the relevant experimental data have proven to be an even more powerful tool.[18−20] In the present study, we utilize a combination of experimental ^{13}C kinetic isotope effects (KIEs) and DFT calculations to probe the rate- and enantioselectivity-determining step of the enantioselective C(sp²)−H alkylation reaction described above. We chose the reaction of 2-benzyl-2-methylcyclopent-4-ene-1,3-dione **1** with either nitromethane (**2a**) or 2-phenylnitroethane (**2b**) catalyzed by **4** for the determination of ^{13}C KIEs at natural abundance. The reaction between **1** and **2b** was used for the determination of intermolecular ^{13}C KIEs[18] by starting material analysis. Accordingly, two independent reactions of **1** and **2b** were taken to 65 ± 2 and 64 ± 2% conversion (in **2b**), and the unreacted **2b** was reisolated for the determination of ^{13}C KIEs. A large normal ^{13}C KIE of ∼1.033 (Figure 1A) was observed on the carbon atom of **2b** bearing the nitro group. This is consistent with either C−C bond formation or the nitro group elimination as the rate-determining step.[21]

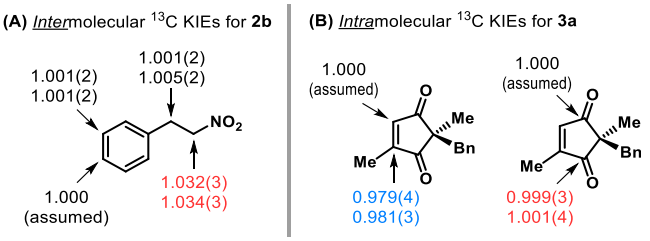

Figure 1. (A) Intermolecular ^{13}C KIEs[18] determined for **2b**. (B) Intramolecular ^{13}C KIEs[19] determined for **3a**. Two sets of KIEs represent independent experiments with six measurements per experiment. Numbers in parentheses show the uncertainty in the last digit of each measurement.

Experimental KIEs for enedione **1** were measured using intramolecular KIE methodology.[19,20] When a symmetric molecule with two identical reaction sites is desymmetrized during a reaction, the ratio of the two isotopomeric products reflects the KIE for the first step that irreversibly desymmetrizes the molecule. At natural abundance, this ratio of isotopomers is obtained by the relative integration of peaks of the two relevant carbon atoms in the ^{13}C NMR spectrum of the product. In the case of symmetric enedione **1**, the intramolecular KIE for the first step that irreversibly desymmetrizes **1** in the catalytic cycle is determined by the relative ^{13}C integration in the NMR spectra of the desymmetrized product **3a**. This intramolecular KIE represents a ratio of isotope effects at the two positions. Accordingly, we determined the intramolecular ^{13}C KIE by quantitative NMR analysis of **3a**, and we observed a significant *inverse* ^{13}C KIE of ∼0.980 on the bond-forming carbon atom of **1** (Figure 1B). Qualitatively, these results rule out conjugate addition of **2a** to **1** as the first irreversible step in the catalytic cycle since this would result in a significant *normal* KIE. Inverse ^{13}C KIEs are typically associated with increased steric crowding at a carbon center. This suggests that one of the steps after the C−C bond formation is the first irreversible step in the catalytic cycle for **1**. Since KIEs for **1** preclude the irreversible C−C bond formation, nitro group elimination emerges as the most likely possibility for the rate- and enantioselectivity-determining step in the catalytic cycle.

To aid in the quantitative interpretation of the experimental KIEs, a DFT study was performed. A thorough potential energy surface scan on all reactants and catalysts was implemented to map the conformational and configurational space for this reaction. B3LYP[22] and B97-D[23,24] (with density fitting) functionals with a def2-SVP basis set[25] and polarized continuum model (IEFPCM)[26,27] were used for geometry optimization and for locating transition structures (TSs). Thermal corrections were calculated using Grimme's quasi-rigid rotor harmonic oscillator approximation.[28] The ^{13}C KIEs were calculated from the scaled vibrational frequencies using the method of Bigeleisen and Mayer[29] as implemented in ISOEFF,[30] and a Wigner tunneling correction[31] was applied. Single point energies were calculated at M06-2X/6-311+G-(d,p)[32,33] using Gaussian 16.[34] Interaction energies were calculated using SAPT0/jun-cc-pVDZ[35−38] as implemented in psi4.[39] This approach has been utilized to evaluate reactivity and selectivity in similar catalytic systems.[40,41] The computa-

https://doi.org/10.1021/jacs.2c02941
J. Am. Chem. Soc. 2022, 144, 17399−17406

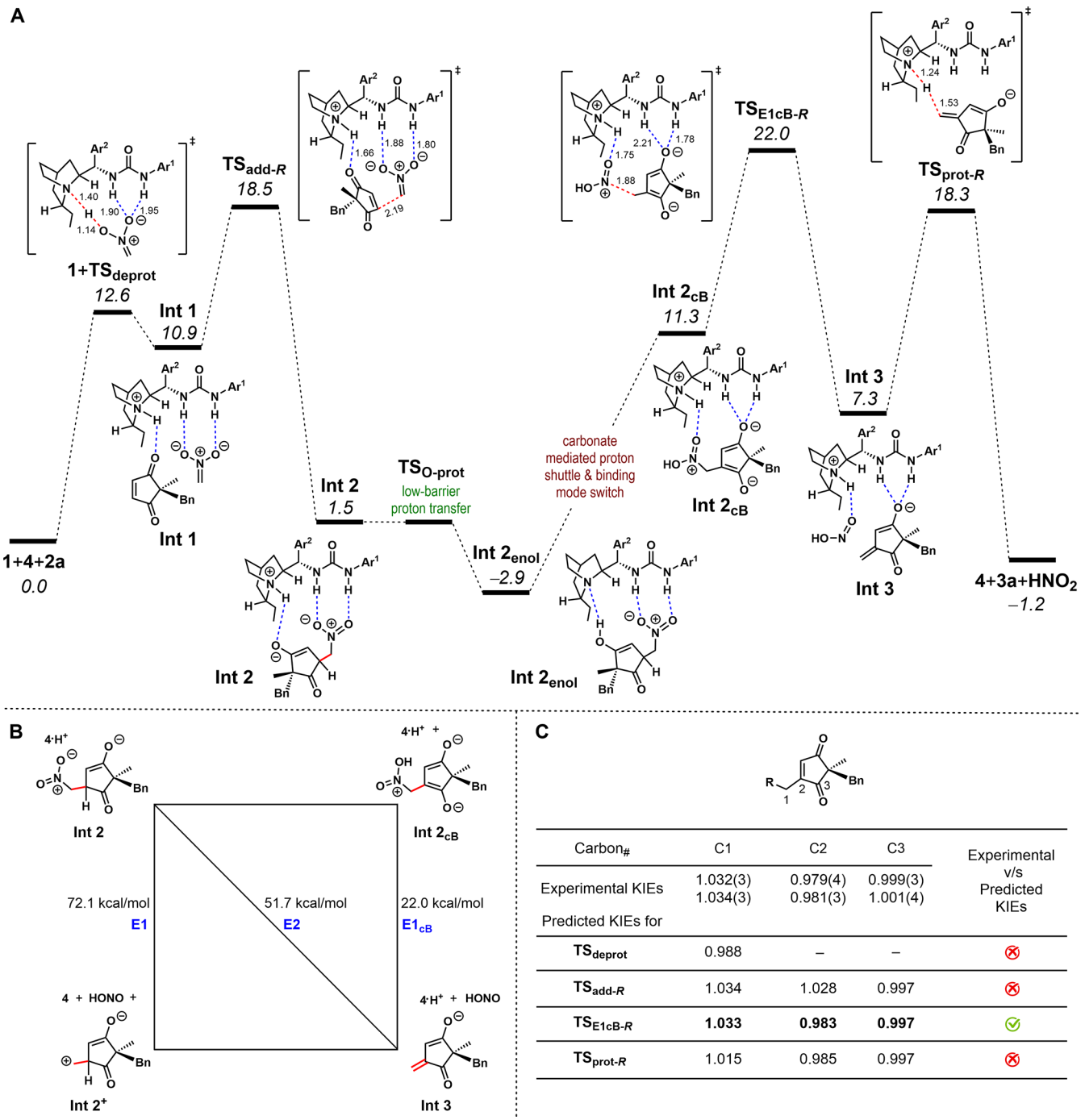

Carbon$_{\#}$	C1	C2	C3	Experimental v/s Predicted KIEs
Experimental KIEs	1.032(3) 1.034(3)	0.979(4) 0.981(3)	0.999(3) 1.001(4)	
Predicted KIEs for				
TS$_{deprot}$	0.988	–	–	⊗
TS$_{add-R}$	1.034	1.028	0.997	⊗
TS$_{E1cB-R}$	**1.033**	**0.983**	**0.997**	✓
TS$_{prot-R}$	1.015	0.985	0.997	⊗

Figure 2. (A) Reaction coordinate diagram for the reaction of **1** and **2a** catalyzed by **4** calculated at the M06-2X/6-311+G(d,p) level of theory. All distances are in angstroms (Å). All energies are shown in kcal/mol and are calculated relative to separate starting materials. (B) More O′ Ferrall-Jencks plot indicating the possible pathways for the conversion of **Int 2** to **Int 3**. (Catalyst structures are omitted for clarity.) (C) Comparison of experimental ^{13}C KIEs and predicted ^{13}C KIEs for each TS along the reaction coordinate. Predictions for C2 and C3 are from TSs shown in Figure 3A, whereas predictions for C1 are from analogous TSs utilizing **2b** instead of **2a** as the alkylating agent.

tional study of this system involved a thorough search of several different reaction pathways and binding modes. A combination of rationally designed transition structures and a conformational search using Grimme's CREST program were utilized to generate 200 unique transition structures which were evaluated energetically and then against the experimentally measured KIEs to determine the most likely mechanistic pathway for the title reaction. (A detailed description of this search is included in the Supporting Information.)

Evaluation of Key Steps in the Reaction Coordinate. The reaction is initiated by deprotonation of **2a** resulting in a protonated catalyst−nitronate complex. The lowest energy TS for this step (Figure 2A, **TS$_{deprot}$**) is stabilized by strong H-bonding interactions of the urea NHs with an oxygen of the nitro group, while the acidic proton of the aci-nitro is deprotonated by the quinuclidine moiety of **4**. The $\Delta G^{\ddagger}$ for **TS$_{deprot}$** is 12.6 kcal/mol relative to separated starting materials. Deprotonation is followed by the conjugate addition

https://doi.org/10.1021/jacs.2c02941
J. Am. Chem. Soc. 2022, 144, 17399−17406

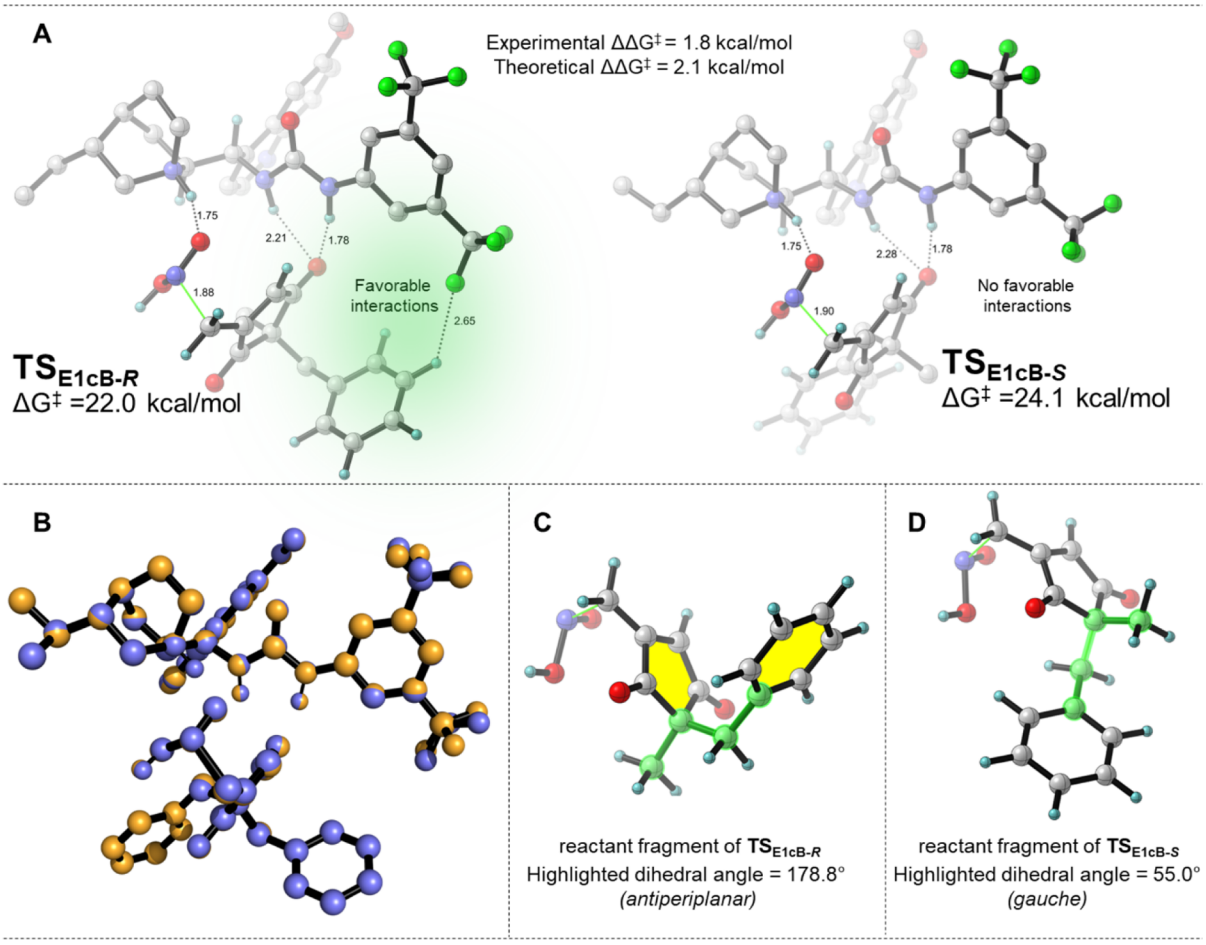

Figure 3. (A) Lowest-energy TSs of the enantioselectivity-determining step for both enantiomers along with experimental and theoretical free-energy barriers. (B) Overlay of the $\mathbf{TS}_{\mathbf{E1cB\text{-}}R}$ (blue) and $\mathbf{TS}_{\mathbf{E1cB\text{-}}S}$ (orange) demonstrating the significant similarities in the catalyst geometry. (C) Separated reactant fragment of $\mathbf{TS}_{\mathbf{E1cB\text{-}}R}$ highlighting the $\pi-\pi$ interaction (yellow) and the antiperiplanar orientation of the phenyl and methyl groups. (D) Separated reactant fragment of $\mathbf{TS}_{\mathbf{E1cB\text{-}}S}$ showing the gauche interaction between the phenyl and methyl groups of the enedione. Molecular graphics were generated using CYLView.[47]

of this nitronate nucleophile to **1**, and the lowest energy TS for this step ($\mathbf{TS}_{\mathbf{add\text{-}}R}$, Figure 2A) leads to the major enantiomer of the product. In this TS, enedione **1** is bound via a strong H-bonding interaction to the protonated quinuclidine (1.66 Å) during conjugate addition of the nitronate, which is bound to the two urea NHs via strong H-bonding interactions (1.88 and 1.80 Å). The developing C−C bond distance in $\mathbf{TS}_{\mathbf{add\text{-}}R}$ is 2.19 Å, and this TS has a $\Delta G^{\ddagger}$ of 18.5 kcal/mol relative to separated starting materials (Figure 2A). Following $\mathbf{TS}_{\mathbf{add\text{-}}R}$, the protonated amine of the cinchona catalyst transfers the proton to the enolate oxygen atom of **Int2** (via $\mathbf{TS}_{\mathbf{O\text{-}prot}}$, a low-barrier proton transfer TS) to form a catalyst-bound enol intermediate $\mathbf{Int2}_{\mathbf{enol}}$. This intermediate, which was found to be 2.9 kcal/mol below separated starting materials, is the catalyst resting state.[42]

Next, we turned our attention to the mechanism of the nitro-elimination step, the likely rate- and enantioselectivity-determining step based on the qualitative interpretation of our experimental KIEs. A More O'Ferrall Jencks plot (Figure 2B) outlines the three possible mechanisms for nitro-elimination from **Int 2** following $\mathbf{TS}_{\mathbf{add\text{-}}R}$. A detailed investigation of the E1 and E2 pathways revealed that these were prohibitively high in energy (72.1 and 51.7 kcal/mol, respectively) and therefore not likely involved in the nitro-elimination from **Int 2** (See pathways 2 and 3 in Supporting Information). Therefore, the most likely mechanism for the nitro-elimination step proceeds via an E1cB pathway. The E1cB mechanism is initiated by deprotonation α to the ketone in $\mathbf{Int\ 2}_{\mathbf{enol}}$ by carbonate to form the conjugate base of $\mathbf{Int\ 2}_{\mathbf{enol}}$ that can then undergo rate-limiting elimination of the nitro group. A thorough investigation revealed that the lowest energy pathway for this elimination event occurs via a dienolate intermediate $\mathbf{Int\ 2}_{\mathbf{cB}}$, which is protonated at the oxygen of the nitro group to make it a good leaving group. Several pathways involving various protonation states and binding modes for E1cB were explored (outlined in pages S23−S39 of the Supporting Information). The pathway outlined in Figure 2A most closely matches the qualitative and quantitative interpretation of the experimental KIEs. Elimination of the protonated nitro group from $\mathbf{Int\ 2}_{\mathbf{cB}}$ (via $\mathbf{TS}_{\mathbf{E1cB\text{-}}R}$) has a $\Delta G^{\ddagger}$ of 22.0 kcal/mol (relative to starting materials),[43] making it the rate- and enantioselectivity-determining step in the catalytic cycle. The intermediate resulting from nitro group elimination (**Int 3**) is protonated via $\mathbf{TS}_{\mathbf{prot\text{-}}R}$ ($\Delta G^{\ddagger}$ = 18.3 kcal/mol relative to starting materials) to deliver product **3a** and regenerate the catalyst.

Predicted KIEs. The relative free energies of the key intermediates and the TSs for the formation of the major product enantiomer (*R*)-**3a** from **1** and **2a** are presented in the

https://doi.org/10.1021/jacs.2c02941
J. Am. Chem. Soc. 2022, 144, 17399−17406

full reaction coordinate (Figure 2A). As conjectured from the qualitative interpretation of our experimental KIEs, nitro group elimination is the first irreversible (highest barrier) step in the catalytic cycle for the reaction between **1** and **2a**. To be consistent with the experiments, all predicted KIEs for **1** are from calculations involving **1** and **2a**, while predicted KIEs for the nitroalkane are from analogous TSs for **2b** (not shown, see the Supporting Information). Predicted KIEs for the first irreversible step in the catalytic cycle should be consistent with the experimental KIE values for both **1** and **2b**. To our satisfaction, excellent agreement between all key experimental KIE values and the corresponding predicted values for $\mathbf{TS}_{\mathbf{E1cB\text{-}}R}$ validated our mechanistic proposal that nitro-elimination via an E1cB pathway is indeed the rate- and enantioselectivity-determining step of the reaction. This conclusion is further supported by the mismatch of experimental and predicted KIEs for **1** and **2b** for all other steps in the reaction pathway (Figure 2C), as well as a KIE mismatch for other higher-energy elimination pathways (see Table S9 in Supporting Information).

Origin of Enantioselectivity. Having established nitro group elimination via $\mathbf{TS}_{\mathbf{E1cB\text{-}}R}$ as the rate- and enantioselectivity-determining step of the reaction, we conducted a detailed conformational search to locate the analogous lowest energy TSs leading to the minor enantiomer of the product [that is, (*S*)-**3a**]. Our explorations resulted in the identification of $\mathbf{TS}_{\mathbf{E1cB\text{-}}S}$, which was found to be 2.1 kcal/mol higher in free energy ($\Delta\Delta G^{\ddagger}$) than $\mathbf{TS}_{\mathbf{E1cB\text{-}}R}$ (Figure 3A). This magnitude of $\Delta\Delta G^{\ddagger}$ corresponds to a predicted er of 98:2 at 263 K, which is in excellent agreement with the experimental er of 97:3 for **3a**. The extent of C−N bond breaking in both the TSs are almost identical (1.88 Å in $\mathbf{TS}_{\mathbf{E1cB\text{-}}R}$ and 1.90 Å in $\mathbf{TS}_{\mathbf{E1cB\text{-}}S}$). Additionally, both $\mathbf{TS}_{\mathbf{E1cB\text{-}}R}$ and $\mathbf{TS}_{\mathbf{E1cB\text{-}}S}$ are stabilized by multiple similar H-bonding interactions: The leaving group (HONO) is H-bonded to the protonated quinuclidine (1.75 Å), while the two thiourea NHs are engaged in stabilization of one of the enolate oxygen atoms. In order to maintain these strong stabilizing interactions, the two substituents at the chiral center (Me and Bn) must switch positions in the two TSs. Consequently, an obvious difference arises, and a moderately stabilizing CH···F interaction (2.65 Å) between one of the aromatic CHs in the benzyl group and one of the CF_3 groups in the catalyst is present only in the TS leading to the major product enantiomer (*R*)-**3a** ($\mathbf{TS}_{\mathbf{E1cB\text{-}}R}$). The importance of CH···F interactions has previously been identified to contribute to selectivity both experimentally and computationally in other thiourea systems.[44,45]

We performed distortion−interaction/activation-strain analysis[46] (DIAC) to decompose the activation energy into strain energy and interaction energy, and to better understand the origin of selectivity. Strain energy is defined as the energy required to distort the ground-state reactants/catalyst into the TS. Interaction energy is defined as the interaction between the distorted catalyst fragment and the reactant fragments in the TS. DIAC decomposed the computed activation energy ($\Delta\Delta E^{\ddagger}$) of 2.8 kcal/mol into 1.2 kcal/mol of strain energy ($\Delta\Delta E_{\mathrm{strain}}^{\ddagger}$) and 1.6 kcal/mol of interaction energy ($\Delta\Delta E_{\mathrm{int}}^{\ddagger}$) favoring the major enantiomer. Overlaying the catalyst fragment from both TSs (Figure 3B) demonstrates the remarkable conformational similarities between the two low-lying diastereomeric TSs (RMSD 0.01 Å, see the Supporting Information, Figure S42). Careful analysis of the reactant conformations reveals numerous differences in the reactant geometries (Figure 3C,D) that contribute to the observed difference in $\Delta\Delta E_{\mathrm{strain}}^{\ddagger}$. Looking down the highlighted C−C bond between the benzylic carbon and the chiral center shows that the phenyl and methyl groups on these adjacent carbon atoms are *anti* to each other in $\mathbf{TS}_{\mathbf{E1cB\text{-}}R}$ (Figure 3C) but are *gauche* to each other in $\mathbf{TS}_{\mathbf{E1cB\text{-}}S}$ (Figure 3D). The antiorientation in $\mathbf{TS}_{\mathbf{E1cB\text{-}}R}$ has the added advantage of stabilizing through CH−π and π-stacking interactions between the phenyl group and the enedione portion of the reactant (yellow highlights Figure 3C). The sterically bulky chiral portion of the catalyst precludes this favorable antiorientation in $\mathbf{TS}_{\mathbf{E1cB\text{-}}S}$.

Finally, fragmentation analysis identified key CH···F interactions present only in the major enantiomer (vide supra). These interactions account for about half of the difference (0.8 kcal/mol) in interaction energies between the competing TSs—demonstrating the importance of the trifluoromethyl groups not only in modulating the acidity of the urea hydrogens but also in providing a stabilizing electrostatic environment for the TS leading to the major enantiomer. The presence of stronger electrostatic interactions in $\mathbf{TS}_{\mathbf{E1cB\text{-}}R}$ (presumably due to shorter urea NH···O distance) accounts for the other half of the interaction energy favoring the major enantiomer. Zeroth-order symmetry-adapted perturbation theory (SAPT0) calculations performed on the TSs further support this hypothesis. SAPT0 analysis reveals the presence of strong electrostatic interactions (+2.6 kcal/mol) between the catalyst monomer fragment and the reactant monomers favoring $\mathbf{TS}_{\mathbf{E1cB\text{-}}R}$. (A complete breakdown of SAPT0 interaction energy can be found in the Supporting Information page S45.) The analysis presented herein identifies all key steric and electronic effects contributing to the observed enantioselectivity in this reaction.

To validate the importance of CH···F interactions identified by the energy decomposition analysis, we synthesized catalyst **5** having methyl groups in place of the CF_3 groups. Catalyst **5** furnished the product (**3a**) with reduced rate and enantioselectivity (93:7 er) compared to that with catalyst **4** (97:3 er) (Scheme 2). We then calculated the lowest-energy transition structures for **5** leading to the two enantiomers of product **3a**. The calculated $\Delta\Delta G^{\ddagger}$ for the reaction catalyzed by **5** is 1.6 kcal/mol, which is 0.5 kcal/mol lower than the corresponding $\Delta\Delta G^{\ddagger}$ for the reaction with **4**. The drop in experimental and computational selectivity with **5** relative to **4** provides proof-of-

Scheme 2. Influence of the Trifluoromethyl Groups in the Catalyst[a]

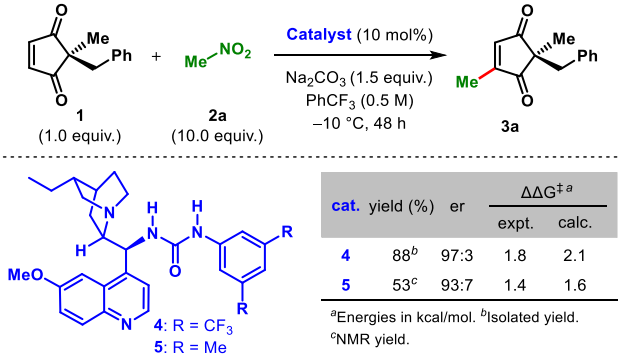

cat.	yield (%)	er	ΔΔG‡ a expt.	ΔΔG‡ a calc.
4	88[b]	97:3	1.8	2.1
5	53[c]	93:7	1.4	1.6

[a]Energies in kcal/mol. [b]Isolated yield. [c]NMR yield.

[a]Boltzmann weighted energies across all TSs.

https://doi.org/10.1021/jacs.2c02941
J. Am. Chem. Soc. 2022, 144, 17399−17406

principle evidence for the importance of CH···F interactions in the selectivity-determining transition states for this reaction.

CONCLUSIONS

We have used a combination of experimental ^{13}C KIEs and DFT calculations to study the mechanism and nature of the rate/enantioselectivity-determining step of the bifunctional tertiary aminourea-catalyzed formal C(sp^2)−H alkylation of cyclopentene-1,3-diones using nitroalkanes as the alkylating agent.[48] Since the chiral center is formed remote from the reaction site, understanding the origin of enantioselectivity is not straightforward. Our studies provide a clear picture of the free-energy profile of the reaction and identifies the elimination of the nitro group as the key step responsible for high enantioselectivity in this reaction. Our results are consistent with nitro group elimination via an E1cB mechanism as the rate- and enantioselectivity-determining step of this reaction. The crucial information that led to this finding is the unusual observation of a large inverse KIE and a large normal KIE on the bond-forming carbon atoms of cyclopentene-1,3-dione and nitroalkane, respectively. Transition state analysis of the diastereomeric TSs identified the main stabilizing interactions as well as conformational effects that dictate the remote stereocontrol. These computational predictions were further supported by experimental observations using a suitably designed catalyst. Accurate evaluation of such complex reaction coordinates is very challenging due to the large errors associated with the energies of steps involving proton transfers relative to the other steps in the catalytic cycle.[49] In this study, experimental ^{13}C KIEs are essential in the evaluation of the free-energy surface (e.g., identification of E1cB step as the first irreversible step) as well as to refine models for explaining selectivity in asymmetric catalysis. Herein, we have demonstrated that heavy-atom KIEs provide a highly precise method for interrogating complex catalytic reaction mechanisms inaccessible solely via computational approaches.[50]

ASSOCIATED CONTENT

Supporting Information

The Supporting Information is available free of charge at https://pubs.acs.org/doi/10.1021/jacs.2c02941.

Experimental details, kinetic measurements, and computational methods (PDF)

Coordinates for all structures (XYZ)

AUTHOR INFORMATION

Corresponding Authors

Santanu Mukherjee − *Department of Organic Chemistry, Indian Institute of Science, Bangalore 560012, India;* orcid.org/0000-0001-9651-6228; Email: sm@iisc.ac.in

Jennifer S. Hirschi − *Department of Chemistry, Binghamton University, Binghamton, New York 13902, United States;* orcid.org/0000-0002-3470-0561; Email: jhirschi@binghamton.edu

Authors

Sharath Chandra Mallojjala − *Department of Chemistry, Binghamton University, Binghamton, New York 13902, United States;* orcid.org/0000-0003-0446-792X

Rahul Sarkar − *Department of Organic Chemistry, Indian Institute of Science, Bangalore 560012, India;* Present Address: Institut für Organische Chemie, Universität Leipzig, Johannisallee 29, D-04103 Leipzig, Germany; orcid.org/0000-0003-3700-6580

Rachael W. Karugu − *Department of Chemistry, Binghamton University, Binghamton, New York 13902, United States*

Madhu Sudan Manna − *Department of Organic Chemistry, Indian Institute of Science, Bangalore 560012, India;* Present Address: Department of Pharmacology, University of Texas Southwestern Medical Center, Dallas, TX-75390, United States.; orcid.org/0000-0003-0364-4947

Sayan Ray − *Department of Organic Chemistry, Indian Institute of Science, Bangalore 560012, India*

Complete contact information is available at: https://pubs.acs.org/10.1021/jacs.2c02941

Author Contributions

The manuscript was written through contributions of all authors. All authors have given approval to the final version of the manuscript. S.C.M. and R.S. contributed equally.

Notes

The authors declare no competing financial interest.

ACKNOWLEDGMENTS

Financial support for this work was provided by Binghamton University startup funds and the National Institutes of Health under R15 GM142103 NIGMS (J.S.H.) and the Science and Engineering Research Board (SERB), India (grant no. EMR/2016/005045) (S.M.). J.S.H. and M.S.C acknowledge support from the XSEDE Science Gateways Program (allocation IDs CHE180061 and CHE210031), which is supported by the National Science Foundation grant number ACI-1548562. R.S. and M.S.M. thank the Council of Scientific and Industrial Research (CSIR), India for their doctoral fellowships. S.R. acknowledges the Ministry of Education, Government of India for his doctoral fellowship through the Prime Minister's Research Fellowship (PMRF) scheme.

REFERENCES

(1) Abrams, D. J.; Provencher, P. A.; Sorensen, E. J. Recent Applications of C−H Functionalization in Complex Natural Product Synthesis. *Chem. Soc. Rev.* **2018**, *47*, 8925−8967.

(2) He, J.; Wasa, M.; Chan, K. S. L.; Shao, Q.; Yu, J. Q. Palladium-Catalyzed Transformations of Alkyl C-H Bonds. *Chem. Rev.* **2017**, *117*, 8754−8786.

(3) Lyons, T. W.; Sanford, M. S. Palladium-Catalyzed Ligand-Directed C−H Functionalization Reactions. *Chem. Rev.* **2010**, *110*, 1147−1169.

(4) Shi, W.; Liu, C.; Lei, A. Transition-Metal Catalyzed Oxidative Cross-Coupling Reactions to Form C-C Bonds Involving Organometallic Reagents as Nucleophiles. *Chem. Soc. Rev.* **2011**, *40*, 2761−2776.

(5) Sambiagio, C.; Schönbauer, D.; Blieck, R.; Dao-Huy, T.; Pototschnig, G.; Schaaf, P.; Wiesinger, T.; Zia, M. F.; Wencel-Delord, J.; Besset, T.; Maes, B. U. W.; Schnürch, M. A Comprehensive Overview of Directing Groups Applied in Metal-Catalysed C−H Functionalisation Chemistry. *Chem. Soc. Rev.* **2018**, *47*, 6603−6743.

(6) Sinha, S. K.; Guin, S.; Maiti, S.; Biswas, J. P.; Porey, S.; Maiti, D. Toolbox for Distal C−H Bond Functionalizations in Organic Molecules. *Chem. Rev.* **2021**, *122*, 5682−5841.

(7) Dutta, U.; Maiti, S.; Bhattacharya, T.; Maiti, D. Arene Diversification Through Distal C(sp^2)−H Functionalization. *Science* **2021**, *372*, eabd5992.

(8) Aynetdinova, D.; Callens, M. C.; Hicks, H. B.; Poh, C. Y. X.; Shennan, B. D. A.; Boyd, A. M.; Lim, Z. H.; Leitch, J. A.; Dixon, D. J. Installing the "Magic Methyl"—C−H Methylation in Synthesis. *Chem. Soc. Rev.* **2021**, *50*, 5517−5563.

(9) Dong, Z.; Ren, Z.; Thompson, S. J.; Xu, Y.; Dong, G. Transition-Metal-Catalyzed C-H Alkylation Using Alkenes. *Chem. Rev.* **2017**, *117*, 9333−9403.
(10) Achar, T. K.; Maiti, S.; Jana, S.; Maiti, D. Transition Metal Catalyzed Enantioselective C(sp^2)−H Bond Functionalization. *ACS Catal.* **2020**, *10*, 13748−13793.
(11) Saint-Denis, T. G.; Zhu, R.-Y.; Chen, G.; Wu, Q.-F.; Yu, J.-Q. Enantioselective C(sp^3)−H Bond Activation by Chiral Transition Metal Catalysts. *Science* **2018**, *359*, eaao4798.
(12) Manna, M. S.; Mukherjee, S. Organocatalytic Enantioselective Formal C(sp^2)−H Alkylation. *J. Am. Chem. Soc.* **2015**, *137*, 130−133.
(13) Sarkar, R.; Mukherjee, S. Catalytic Enantioselective Desymmetrization of Norbornenoquinones via C(sp^2)−H Alkylation. *Org. Lett.* **2016**, *18*, 6160−6163.
(14) Ray, S.; Mondal, S.; Mukherjee, S. Enantioselective Total Synthesis of [3]-Ladderanol through Late-Stage Organocatalytic Desymmetrization. *Angew. Chem., Int. Ed.* **2022**, *61*, e202201584.
(15) Metrano, A. J.; Miller, S. J. Peptide-Based Catalysts Reach the Outer Sphere through Remote Desymmetrization and Atroposelectivity. *Acc. Chem. Res.* **2019**, *52*, 199−215.
(16) Choudhury, A. R.; Manna, M. S.; Mukherjee, S. Nitro-Enabled Catalytic Enantioselective Formal Umpolung Alkenylation of beta-Ketoesters. *Chem. Sci.* **2017**, *8*, 6686−6690.
(17) Li, Y.; Ibsen, L.; Jørgensen, K. A. Formal Asymmetric alpha-Alkenylation of Aldehydes and the Synthetic Application toward Forming alpha-exo-Methylene-gamma-butyrolactones and Skipped Dienes. *Org. Lett.* **2017**, *19*, 1200−1203.
(18) Singleton, D. A.; Thomas, A. A. High-Precision Simultaneous Determination of Multiple Small Kinetic Isotope Effects at Natural Abundance. *J. Am. Chem. Soc.* **1995**, *117*, 9357−9358.
(19) Singleton, D. A.; Szymanski, M. J. Simultaneous Determination of Intermolecular and Intramolecular ^{13}C and ^{2}H Kinetic Isotope Effects at Natural Abundance. *J. Am. Chem. Soc.* **1999**, *121*, 9455−9456.
(20) Wambua, V.; Hirschi, J. S.; Vetticatt, M. J. Rapid Evaluation of the Mechanism of Buchwald−Hartwig Amination and Aldol Reactions Using Intramolecular ^{13}C Kinetic Isotope Effects. *ACS Catal.* **2020**, *11*, 60−67.
(21) The isomerization step also involves this carbon atom; however, protonation steps are typically associated with smaller ^{13}C KIEs than observed experimentally.
(22) Becke, A. D. Density-functional thermochemistry. III. The role of exact exchange. *J. Chem. Phys.* **1993**, *98*, 5648−5652.
(23) Grimme, S. Semiempirical GGA-type Density Functional Constructed with a Long-Range Dispersion Correction. *J. Comput. Chem.* **2006**, *27*, 1787−1799.
(24) Becke, A. Density-Functional Thermochemistry. V. Systematic Optimization of Exchange-Correlation Functionals. *J. Chem. Phys.* **1997**, *107*, 8554−8560.
(25) Weigend, F.; Ahlrichs, R. Balanced Basis Sets of Split Valence, Triple Zeta Valence and Quadruple Zeta Valence Quality for H to Rn: Design and Assessment of Accuracy. *Phys. Chem. Chem. Phys.* **2005**, *7*, 3297−3305.
(26) Miertuš, S.; Scrocco, E.; Tomasi, J. Electrostatic Interaction of a Solute with a Continuum—a Direct Utilization of Abinitio Molecular Potentials for the Prevision of Solvent Effects. *Chem. Phys.* **1981**, *55*, 117−129.
(27) Tomasi, J.; Mennucci, B.; Cammi, R. Quantum Mechanical Continuum Solvation Models. *Chem. Rev.* **2005**, *105*, 2999−3094.
(28) Ribeiro, R. F.; Marenich, A. V.; Cramer, C. J.; Truhlar, D. G. Use of Solution-Phase Vibrational Frequencies in Continuum Models for the Free Energy of Solvation. *J. Phys. Chem. B* **2011**, *115*, 14556−14562.
(29) Bigeleisen, J.; Mayer, M. G. Calculation of Equilibrium Constants for Isotopic Exchange Reactions. *J. Chem. Phys.* **1947**, *15*, 261−267.
(30) Anisimov, V.; Paneth, P. A Program for Studies of Isotope Effects Using Hessian Modifications. *J. Math. Chem.* **1999**, *26*, 75−86.
(31) Wigner, E. Über das Überschreiten von Potentialschwellen bei chemischen Reaktionen. *Z. Phys. Chem., Abt. B* **1932**, *19*, 203.
(32) Zhao, Y.; Truhlar, D. G. The M06 Suite of Density Functionals for Main Group Thermochemistry, Thermochemical Kinetics, Noncovalent Interactions, Excited States, and Transition Elements: Two New Functionals and Systematic Testing of Four M06-Class Functionals and 12 Other Functionals. *Theor. Chem. Acc.* **2008**, *120*, 215−241.
(33) Hehre, W. J.; Stewart, R. F.; Pople, J. A. Self-Consistent Molecular-Orbital Methods. I. Use of Gaussian Expansions of Slater-Type Atomic Orbitals. *J. Chem. Phys.* **1969**, *51*, 2657−2664.
(34) Frisch, M. J.; Trucks, G. W.; Schlegel, H. B.; Scuseria, G. E.; Robb, M. A.; Cheeseman, J. R.; Scalmani, G.; Barone, V.; Petersson, G. A.; Nakatsuji, H.; Li, X.; Caricato, M.; Marenich, A. V.; Bloino, J.; Janesko, B. G.; Gomperts, R.; Mennucci, B.; Hratchian, H. P.; Ortiz, J. V.; Izmaylov, A. F.; Sonnenberg, J. L.; Williams; Ding, F.; Lipparini, F.; Egidi, F.; Goings, J.; Peng, B.; Petrone, A.; Henderson, T.; Ranasinghe, D.; Zakrzewski, V. G.; Gao, J.; Rega, N.; Zheng, G.; Liang, W.; Hada, M.; Ehara, M.; Toyota, K.; Fukuda, R.; Hasegawa, J.; Ishida, M.; Nakajima, T.; Honda, Y.; Kitao, O.; Nakai, H.; Vreven, T.; Throssell, K.; Montgomery, J. A., Jr.; Peralta, J. E.; Ogliaro, F.; Bearpark, M. J.; Heyd, J. J.; Brothers, E. N.; Kudin, K. N.; Staroverov, V. N.; Keith, T. A.; Kobayashi, R.; Normand, J.; Raghavachari, K.; Rendell, A. P.; Burant, J. C.; Iyengar, S. S.; Tomasi, J.; Cossi, M.; Millam, J. M.; Klene, M.; Adamo, C.; Cammi, R.; Ochterski, J. W.; Martin, R. L.; Morokuma, K.; Farkas, O.; Foresman, J. B.; Fox, D. J. *Gaussian 16*; Rev. C.01: Wallingford, CT, 2016.
(35) Jeziorski, B.; Moszynski, R.; Szalewicz, K. Perturbation-Theory Approach to Intermolecular Potential-Energy Surfaces of Van-Der-Waals Complexes. *Chem. Rev.* **1994**, *94*, 1887−1930.
(36) Szalewicz, K. Symmetry-Adapted Perturbation Theory of Intermolecular Forces. *Wiley Interdiscip. Rev. Comput. Mol. Sci.* **2012**, *2*, 254−272.
(37) Hohenstein, E. G.; Sherrill, C. D. Density Fitting of Intramonomer Correlation Effects in Symmetry-Adapted Perturbation Theory. *J. Chem. Phys.* **2010**, *133*, 014101.
(38) Hohenstein, E. G.; Sherrill, C. D. Density Fitting and Cholesky Decomposition Approximations in Symmetry-Adapted Perturbation Theory: Implementation and Application to Probe the Nature of $\pi-\pi$ Interactions in Linear Acenes. *J. Chem. Phys.* **2010**, *132*, 184111.
(39) Turney, J. M.; Simmonett, A. C.; Parrish, R. M.; Hohenstein, E. G.; Evangelista, F. A.; Fermann, J. T.; Mintz, B. J.; Burns, L. A.; Wilke, J. J.; Abrams, M. L.; Russ, N. J.; Leininger, M. L.; Janssen, C. L.; Seidl, E. T.; Allen, W. D.; Schaefer, H. F.; King, R. A.; Valeev, E. F.; Sherrill, C. D.; Crawford, T. D. PSI4: An Open-Source *ab initio* Electronic Structure Program. *Wiley Interdiscip. Rev. Comput. Mol. Sci.* **2012**, *2*, 556−565.
(40) Lam, Y. H.; Grayson, M. N.; Holland, M. C.; Simon, A.; Houk, K. N. Theory and Modeling of Asymmetric Catalytic Reactions. *Acc. Chem. Res.* **2016**, *49*, 750−762.
(41) Peng, Q.; Duarte, F.; Paton, R. S. Computing organic stereoselectivity—from concepts to quantitative calculations and predictions. *Chem. Soc. Rev.* **2016**, *45*, 6093−6107.
(42) We also modeled the transition state for C-protonation of **Int 2** to yield the keto-form of **Int 2**$_{enol}$ and found this TS to be >10 kcal/mol higher in energy than the O-protonation TS. The catalyst-bound keto intermediate is 6.3 kcal/mol higher in energy than **Int 2**$_{enol}$. See Supporting Information for the full description of these calculations.
(43) The estimated half life based on Gibbs-Eyring equation for a free energy barrier of 21.5 kcal/mol for a unimolecular reaction at 263 K with a transmission coefficient of 1 is 1.07 days. The reported reaction takes about 48 h for completion.
(44) Singh, S.; Sunoj, R. B. Computational asymmetric catalysis: On the origin of stereoselectivity in catalytic reactions. *Advances in Physical Organic Chemistry*; Williams, I. H., Williams, N. H., Eds.; Academic Press, 2019; Vol. 53, Chapter 1, pp 1−27.
(45) Bhaskararao, B.; Sunoj, R. B. Two chiral catalysts in action: insights into cooperativity and stereoselectivity in proline and

https://doi.org/10.1021/jacs.2c02941
J. Am. Chem. Soc. 2022, 144, 17399−17406

cinchona-thiourea dual organocatalysis. *Chem. Sci.* **2018**, *9*, 8738−8747.
(46) Bickelhaupt, F. M.; Houk, K. N. Analyzing Reaction Rates with the Distortion/Interaction-Activation Strain Model. *Angew. Chem., Int. Ed.* **2017**, *56*, 10070−10086.
(47) Legault, C. Y. *CYLview, 1.0b*; Université de Sherbrooke, 2009. http://www.cylview.org.
(48) An earlier version of this manuscript was deposited on ChemRxiv on 01 October 2021 Mallojjala, S. C.; Sakar, R.; Karugu, R. W.; Manna, M. S.; Mukherjee, S.; Hirschi, J. S. Mechanism and Origin of Remote Stereocontrol in the Organocatalytic C(sp2)-H Alkylation using Nitroalkanes as Alkylating Agents. *Catalysis* **2021**, DOI: 10.26434/chemrxiv-2021-x5mkp.
(49) Plata, R. E.; Singleton, D. A. A Case Study of the Mechanism of Alcohol-Mediated Morita-Baylis-Hillman Reactions. The Importance of Experimental Observations. *J. Am. Chem. Soc.* **2015**, *137*, 3811−3826.
(50) Dale, H. J. A.; Leach, A. G.; Lloyd-Jones, G. C. Heavy-Atom Kinetic Isotope Effects: Primary Interest or Zero Point? *J. Am. Chem. Soc.* **2021**, *143*, 21079−21099.

https://doi.org/10.1021/jacs.2c02941
J. Am. Chem. Soc. 2022, 144, 17399−17406